Metamorphic characteristics and geotectonic implications of the high-pressure granulites from Namjagbarwa, eastern Tibet*

DING Lin (丁 林) and ZHONG Dalai (钟大赉)

(Institute of Geology, Chinese Academy of Sciences, Beijing 100029, China)

Received March 16, 1999

Abstract A large area of high-pressure garnet-kyanite granulite is exhumed in the Namjagbarwa area, which provides a window for observing the deep crust rocks and structures of the Tibetan Plateau. Three mineral assemblages can have been distinguished in the garnet-kyanite HP granulites by petrography, i.e. M_1. Mus + Bi + Pl + Q, M_2. Gt + Ky + perphite/antiperphite + Rt + Q, M_3. Gt + Sill + Cord + Sp + Ilm ± Opx. Metamorphic conditions of the peak granulite assemblages (M_2) formatted by thickening of crusts, with available isotopic ages of 45—69 Ma, are at 1.4—1.8 Gpa and 750—850℃. Their retrograde assemblages overprinted by decompressure during the uplift, with available isotopic ages of 18—23 Ma, were formed at 0.60—0.70 Gpa, 621—726℃. The thermobarometric evaluation, petrogenetic grid and corresponding isotopic ages indicate a clockwise isothermal decompression metamorphic path. The HP granulite metamorphic history indicates that the collision of the Indian Plate with the Eurasian Plate had begun at 70 Ma, far earlier than the widely accepted 45 Ma.

Keywords: Tibetan Plateau, Namjagbarwa, HP granulite, metamorphism.

1 Geological setting

Namjagbarwa, located on the inside of the Yarlung Zangbo River bend of the eastern Himalayan syntaxis (EHS), is the highest peak of the eastern Himalayan Mountains. The geographical and geological boundaries of the EHS have been bent around the Namjagbarwa Mountains resulting from the indention of the northeastern corner of the Indian Plate since the collision of the Indian Plate and the Eurasian Plate (fig. 1). With the tectonic thickening and rapid exhuming, a large area of HP granulites is outcropped, which provided a window for observing the deep crust rocks and structures of the Tibetan Plateau[1,2].

At one time, these metamorphic rocks exhumed in these areas were called the Namjagbarwa group, which was thought to have experienced greenschist to amphibolite facies metamorphism[3,4]. In recent years, a large area of granulite facies metamorphic rocks along with some granite, granodiorite, diorite and gabbro have been found in the center of the EHS by our own mapping (figure 1).

The HP granulites, which occurred along the Pai strike-slip fault in the western side of the Namjagbarwa, contact with the country rock by mylonitic zone with the same strikes as the area gneissosity (fig. 1). The country rocks of the HP granulites are sillimanite-garnet gneisses, granitic gneisses, and biotite gneisses. The main type of the HP granulites is garnet-kyanite granulite, the other is some HP clinopyroxene-garnet granulite which was enclosed as lens or uncontinuous ribbon in

* Project supported by the National Natural Science Foundation of China (Grant No. 49732100), the National Key Project for Basic Research, and the Chinese Academy of Sciences Project for Tibetan Research Project (Grant Nos. KZ951-A1-204, KZ95T-06).

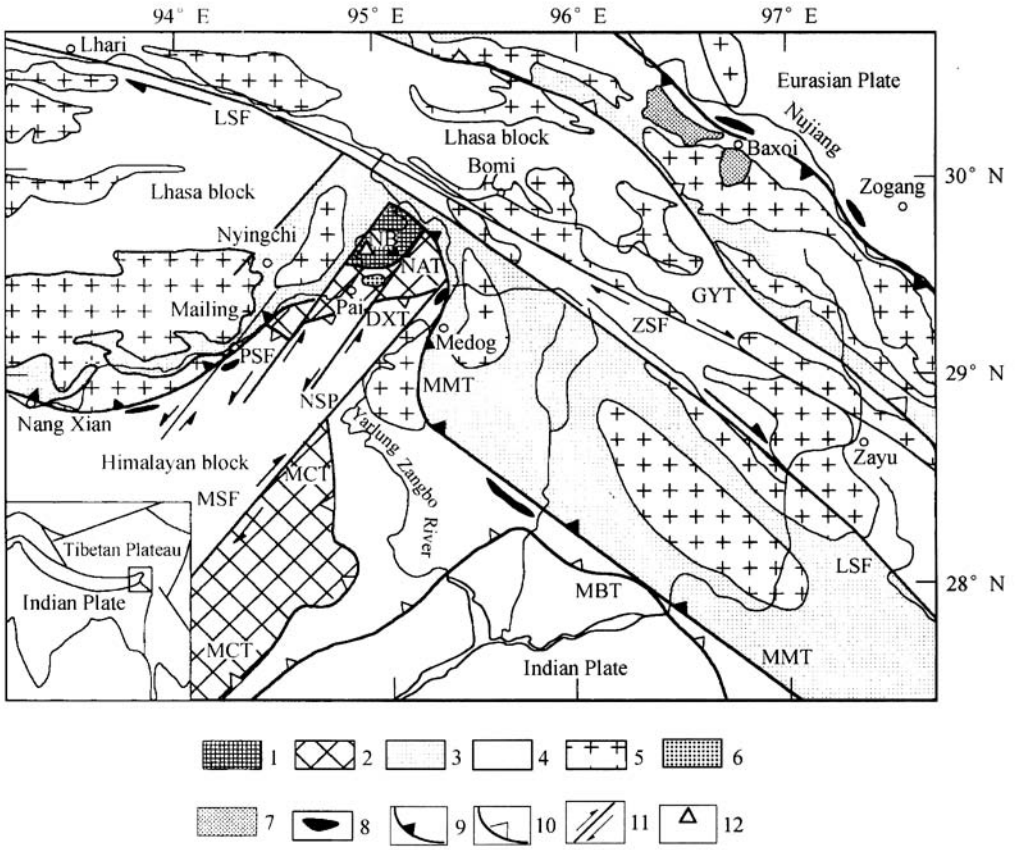

Fig. 1. Simple tectonic map of the Eastern Himalayan Syntaxis. 1, Granulite rocks; 2, High Himalayan crystalline series; 3, Gangdise metamorphic basement; 4, Paleozoic-Mesozoic stratigraphy; 5, Gangdise arc granites; 6, Diorite-gabbroes of Namla Co; 7, Gangdise arc volcanic rocks; 8, ophilites; 9, suture zone; 10, large-scale thrust; 11, strike-slip fault; 12, sample location. DXT, Duoxiongla thrust; GYT, Guyu thrust; LSF, Lhari strike-slip fault; MBT, main boundary thrust; MCT, main central thrust; MMT, main mantle thrust; MSF, Medog strike-slip fault; NAT, Nanao thrust; NB, Namjagbarwa mountain; NSF, Nage strike-slip fault; PSF, Pai strike-slip fault; ZSF, Zayu strike-slip fault.

the garnet-kyanite HP granulite[2]. In this paper, we focus our attention on the metamorphism of the HP garnet-kyanite granulite and its geotectonic significance.

2 Petrography

Garnet-kyanite granulites show gray-white color, gneissic structure and porphyroblastic texture. The porphyroblastes are garnets, kyanites and sillimanites with grainsizes ranging 1—10 mm in their long axis. Garnet porphyroblastes often show a diablastic texture in their center which include inclusions of biotites, rutiles, kyanites, quartzes (fig. 2(a)). Tubular-prismatic kyanite porphyroblastes present a poikilitic texture with inclusions of muscovites, biotites, quartzes and rutiles (fig. 2(b) and (c)). Matrix, composed of plagioclases, orthoclases, quartzes, biotites and sillimanites respectively, are medium- to coarse-grained subhedral porphyroblastes texture with size range of 1—5 mm. A prominent foliation is defined by the alignment of coarse prisms of sillimanites and scale-aggregate bi-

otites.

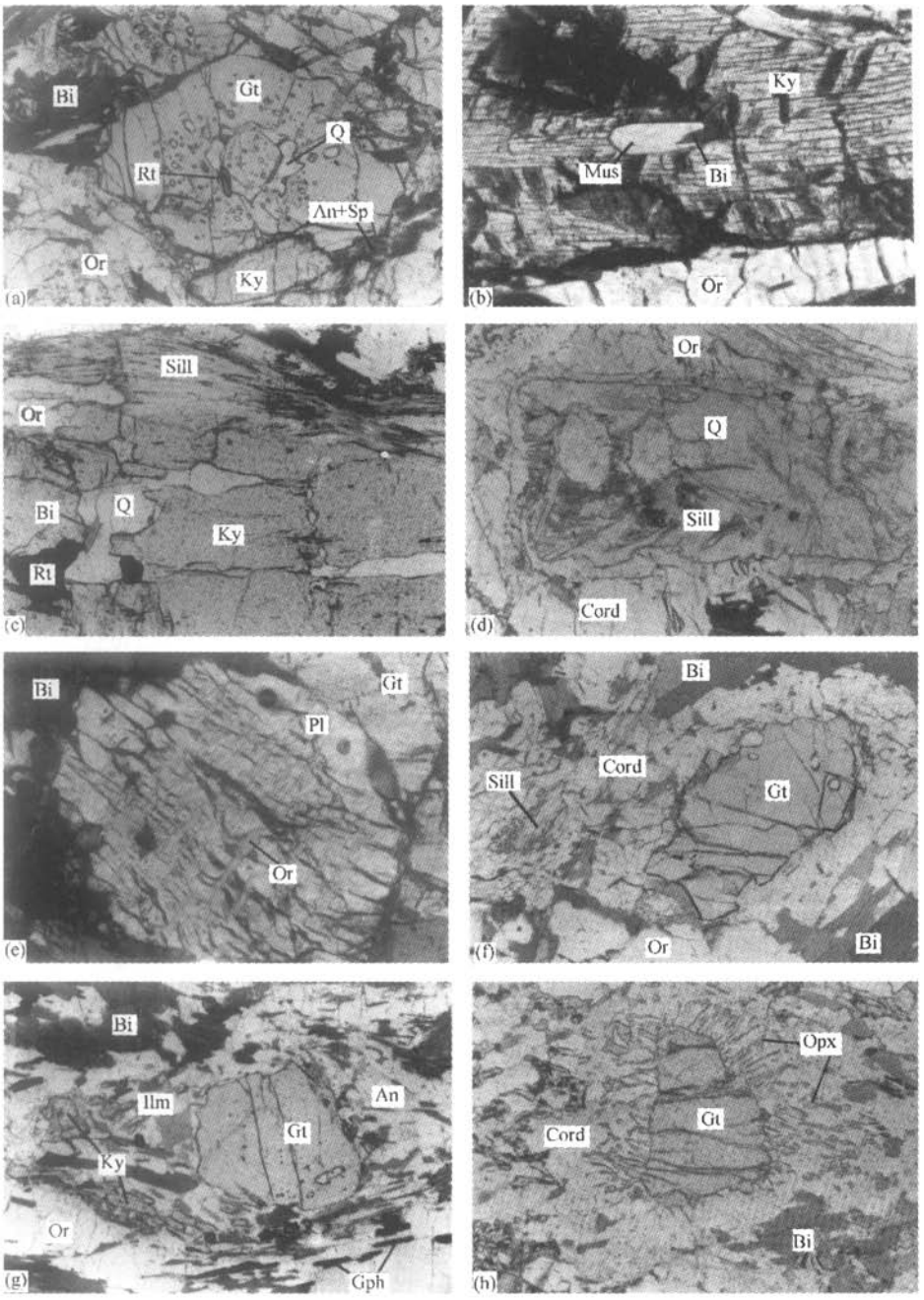

(*To be continued on the next page*)

(*Continued*)

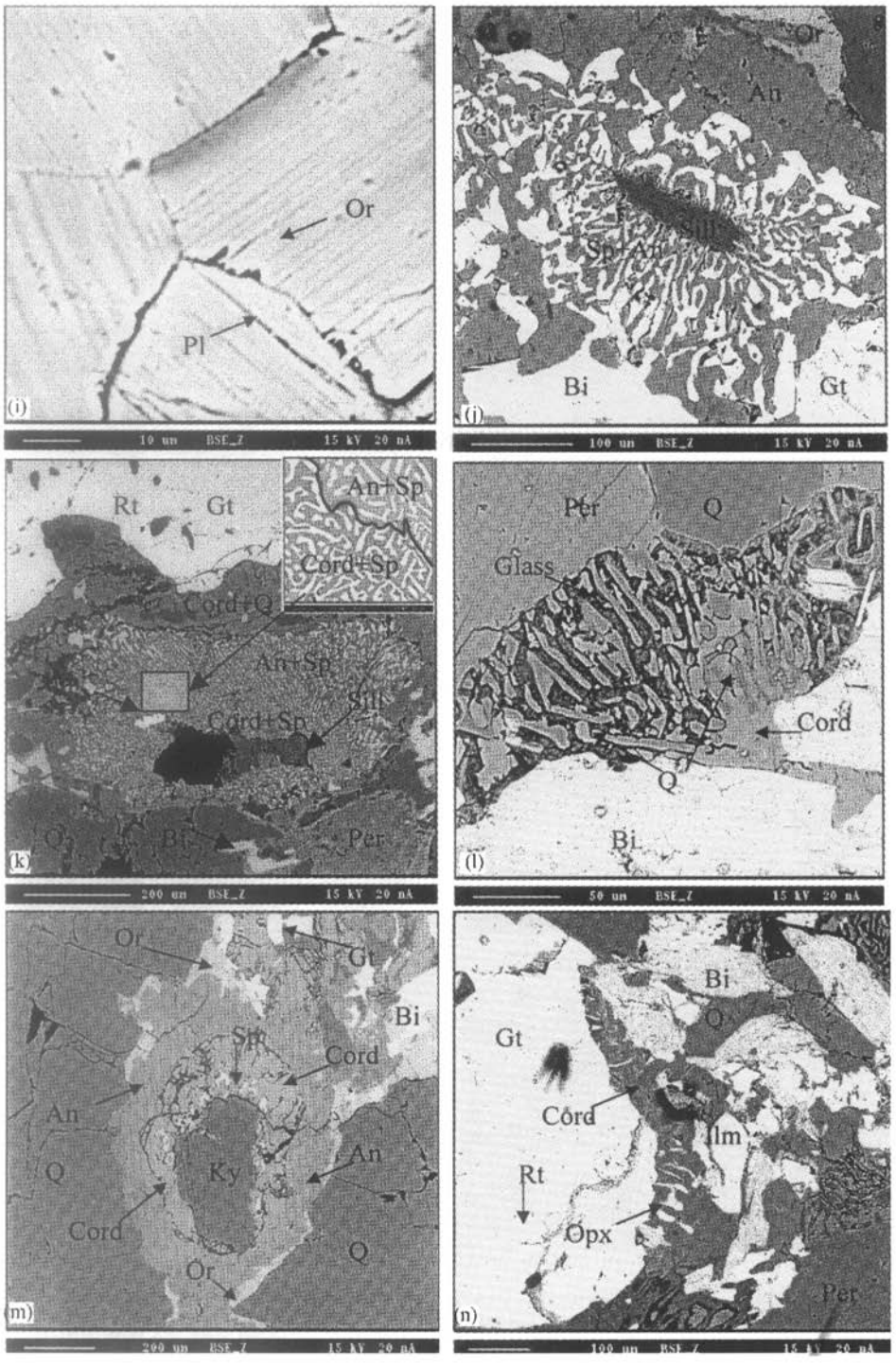
Or
Pl
(i)
10 um BSE_Z 15 kV 20 nA
Or
An
Sill
Sp+An
Bi
Gt
(j)
100 um BSE_Z 15 kV 20 nA
Rt
Gt
An+Sp
Cord+Sp
Cord+Q
An+Sp
Sill
Cord+Sp
Bi
Per
(k)
200 um BSE_Z 15 kV 20 nA
Per
Q
Glass
Cord
Q
Bi
(l)
50 um BSE_Z 15 kV 20 nA
Or
Gt
Bi
Sill
Cord
An
Q
Ky
An
Cord
Q
Or
(m)
200 um BSE_Z 15 kV 20 nA
Bi
Q
Gt
Cord
Ilm
Rt
Opx
Per
(n)
100 um BSE_Z 15 kV 20 nA

Fig. 2. Mineral reaction textures in HP granulites from Namjagbarwa. (a) Garnet porphyroblaste with a diablastic center and clear rim, the inclusions are quartz, plagioclase and rutile respectively; (b) kyanite porphyroblaste with inclusions of muscovite and biotite; (c) kyanite porphyroblastes co-existing with orthoclase. The rim of the kyanite is directly replaced by sillimanites; (d) prismatic sillimanite aggregations with a cordierite coronas, which show a kyanite tubular peseudoform; (e) antiperthite porphyroblaste; (f) Cord + Q coronas between garnet and sillimanite; (g) An + Bi coronas replacing garnet and kyanite porphyroblastes; (h) Cord + Opx coronas mantling garnet porphyroblaste; (i) micro-alkali perthites showing triple junction texture formatted during the high temperature and pressure granulite metamorphic stage; (j) Sp + An symplectites replacing sillimanite (kyanite peseudoform); (k) Sp + Cord, Sp + An and Cord + Q symplectites between garnet and sillimanite (kyanite peseudoform) porphyroblastes. Sp + Cord symplectites mantling the sillimanite porphyroblaste, Cord + Q symplectites mantling the garnet porphyroblaste, and the Sp + An symplectites setting between the Sp + Cord and the Cord + Q symplectites. Inset: the detail of the relation of the two stages of symplectites, Sp + An and Sp + Cord; (l) partial melting at the triple junction of biotite quartz and antiperthite, which shows a quenching texture of intergrowthing of cordierites, quartz wormform crystals and glass; (m) multiple phases of coronas rimming the kyanite porphyroblaste. The peak assemblages of Ky + Per are divided by early anorthite coronas, and the late Cord + Sp coronas also replacing the earlier anorthite coronas; (n) Opx + Cord symplectites replacing the garnet porphyroblastes.

Reaction textures and pretrography observed in the HP granulites of these areas show that the minerals can be subdivided into early, middle and late metamorphic assemblages on the textural relations.

The early metamorphic assemblages (M_1) are characterized by relic inclusions of Mus + Bi + Pl + Q in garnet and kyanite porphyroblastes (fig. 2(a)—(c)). Most of the relic muscovite crystals are phengites (Si = 3.28—3.35), which commonly occur in kyanite porphyroblastes, showing elliptical shape with long axis up to 0.2 mm, perfect basal cleavage, nearly parallel extinction and biaxial-negative character with 30°—40° of their 2V (figure 2(b)).

The middle metamorphic assemblages (M_2), which represent the high temperature and pressure granulite assemblages, are characterized by porphyroblastic crystals such as garnets, kyanites, perthites or antiperthites, rutiles and quartzes with accessory minerals such as corundum, zircons, graphites, apatites, monazites and xenotimes. Tubular-prismtic kyanites are light blue, have well-developed cleavage and prominent parting parallel to (001). Kyanites are easily recognized by their first-order gray to orange interference colors, simple twinning, oblique extinction with 20°—30°, and biaxial-negative character with 30°—40° of their 2V (figure 2(c), (g) and (m)).

The late metamorphic assemblage (M_3), Sill + Gt + Bi + Pl ± Cord ± Opx, are characterized by the polymineralic coronas rimming the peak metamorphic minerals. Kyanites, garnets, perthites and rutiles have their own unique corona textures. In some cases, kyanite is partially or completely replaced by sillimanite, although the kyanite crystal forms are retained (fig. 2 (d), (j) and (k)). Whereas other kyanites are replaced by the symplectis or coronas of anorthites and spinels, and sillimanites are ulteriorly replaced by cordierites, and no co-existing of quartz and spinel is found in the coronas.

$$Py + 12Ky + 5Gr = 15An + 3Sp, \quad (1)$$

$$Ky = Sill, \quad (2)$$

$$2Sill + Py = Sp + Cord. \quad (3)$$

There are at least three types of coronas that occur at the rim of garnet porphyroblastes in different samples and garnets, such as Cord + Q, An ± Bi and Cord + Opx (fig. 2(f), (g), (h) and (n)).

$$Gr + 2Ky + Q = 3An, \quad (4)$$

$$2Py + 4Ky/Sill + 5Q = 3Cord, \quad (5)$$

$$2Py + 3Q = 2Opx + Cord. \quad (6)$$

Rutiles that occur as inclusions in garnet or kyanite porphyroblastes or as isolated crystals in ma-

trix are mantled by Ilmenites. So the rutiles coexist with peak metamorphic assemblages (fig. 2(a) and (c)),

$$\mathrm{Alm} + 3\mathrm{Rt} = 2\mathrm{Q} + \mathrm{Ky} + 3\mathrm{Ilm}. \quad (7)$$

The single-phase ternary feldspar[5] of the high temperature assemblages usually breaks down into separate orthoclases and oligoclase lamellas during the retrogression, and behaves as perthites or antiperthites (fig. 2(e) and (i)). In some samples, partial melt occurs at triple junction with the intergrowthing of cordierite, wormform quartz and glass (figure 2(l)).

3 Mineral chemistry

Representative analyses of the minerals are presented in table 1. Minerals were analyzed using an CAMECAS-51 electron-microprobe at the Institute of Geology, Chinese Academy of Sciences, operating with an accelerating voltage of 15 kV, electric current of 20 nA, and a beam width of 5—10 μm.

Garnet porphyroblastes of the HP granulite of these areas are almandine-, pyrope-rich, and grossular-, spessartine-poor (table 1, figure 3).

The end-members range 60%—70% for almandine, 10%—29% for pyrope, 0%—13% for grossular and 1%—15% for spessartine. The f/m (f/m = 100 (Fe + Mn)/(Fe + Mg + Mn)) ration range from 0.72 to 0.90. Compositional profiles across garnet prophyroblastes were automaticly measured by the electric-probe at equidistant intervals from rim to rim through the core per sample (fig. 3). All of the garnet prophyroblastes are unzoned except near their rims which have been formatted by retrogression. Almandine, pyrope, grossular, spessartine and f/m ratio are constant in the interior of garnet porphyroblastes. However, the end-members are abruptly changed at 100—300 μm from rim. Almandine, spessartin and f/m significant increase, and grossular and pyrope synchronously drop to the rim, suggesting that the rocks have suffered a rapid decompressing metamorphism[6,7]. It may be that early stage garnet in the core of one large garnet prophyroblastes is (95T134) characterized by higher f/m ration and lower grossular compared with the garnet of peak granulite assemblages. Its end-member is $\mathrm{Alm}_{62.4}\mathrm{Spe}_{4.4}\mathrm{Pyr}_{23.5}\mathrm{Gro}_{7.3}$.

In some HP granulite samples 94T12, 94T26 and 95T134 only microantiperthite occurs, but in other samples (95T146) both microantiperthites and microperthites appear. For the antiperthites, they exist as porphyroclasts or inclusions with grainsize of 1—10 mm. Their contents range from 1% to 10% in different samples. The plagioclases are oligoclases to andesines (table 1) which range from 27.2% to 40.2% for anorthites, from 2.3% to 5.2% for orthoclases, and from 57.2% to 69.8% for albites. Within the pudding or flame shape lamellas are potassium-rich feldspars which range from 0.3% to 0.7% for anorthites, from 61.4% to 92.0% for orthoclase, and from 7.7% to 37.7% for albites. The composition of the high temperature single-phase feldspars, which has been determined on the line scan analysis across the antiperthite grains in all the samples discussed, range from 26% to 38% for anorthite, from 6.8% to 10.6% for orthoclase, and from 55.1% to 67.1% for albite. Microperthites occur in sample 95T146, with the host crystal feldspars 0.3% for anorthite, 75.1% for orthoclase, and 24.6% for albite. And the thin straight exsolution lamellaes are oligoclases that are 26.4% for anorthite, 2.3% for orthoclase, and 71.4% for albite. The high temperature single-phase alkali-feldspars determined by the line scan analysis across the microperthite grains is 2.3% for anorthite,

Table 1 Mineral microprobe analysis of garnet-kyanite granulite samples from Namjagbarwa

Minerals	Garnet								Biotite							
Specimen	94t12		94t26		95T134		95t146		94t12		94t26		95t134		95t146	
Location	core	rim	core	rim	core	rim	core	rim	core	rim	core	rim	core	rim	core	rim
SiO_2	38.18	37.50	38.21	37.45	37.68	37.19	37.05	37.52	36.41	35.85	35.15	35.27	36.59	35.73	35.97	36.55
TiO_2	0.01	0.06	0.00	0.02	0.02	0.04	0.08	0.09	5.41	4.39	6.67	3.66	5.51	4.61	5.43	4.97
Al_2O_3	21.30	21.06	21.12	21.11	21.29	20.82	21.42	21.07	16.89	19.33	17.47	17.09	16.99	17.30	16.55	17.08
Cr_2O_3	0.06	0.08	0.07	0.03	0.00	0.02	0.01	0.04	0.01	0.07	0.00	0.16	0.07	0.14	0.15	0.02
Fe_2O_3	0.59	0.42	0.76	0.34	0.51	0.56	0.52	0.00								
MgO	6.41	5.50	5.01	4.49	6.10	4.31	6.16	5.89	12.42	12.01	9.49	11.32	12.23	12.25	12.13	12.91
CaO	3.42	2.06	4.54	2.51	5.19	3.41	2.82	0.84	0.00	0.00	0.00	0.00	0.02	0.00	0.00	0.00
MnO	2.05	1.01	0.56	1.51	0.93	1.65	1.01	1.43	0.05	0.04	0.00	0.05	0.00	0.07	0.00	0.07
FeO	28.30	32.10	30.28	32.54	27.91	31.42	31.02	32.46	14.72	13.87	16.39	18.67	15.57	17.51	16.44	14.38
NiO	0.01	0.05	0.05	0.02	0.00	0.04	0.00	0.05	0.04	0.00	0.02	0.01	0.05	0.00	0.12	0.09
Na_2O	0.00	0.03	0.09	0.09	0.00	0.00	0.02	0.05	0.22	0.51	0.21	0.18	0.24	0.22	0.17	0.18
K_2O	0.00	0.02	0.00	0.01	0.02	0.03	0.00	0.05	9.20	9.42	9.17	8.78	8.71	8.75	9.20	9.58
H_2O									4.03	4.05	3.96	4.07	4.05	3.91	4.02	4.05
Total	100.3	99.89	100.7	100.1	99.66	99.48	100.1	99.54	99.41	99.54	98.54	99.34	100.0	100.5	100.2	99.89
O	24	24	24	24	24	24	24	24	24	24	24	24	24	24	24	24
Si	5.97	5.96	6.00	5.97	5.93	5.96	5.91	5.89	5.42	5.31	5.33	5.47	5.41	5.33	5.37	5.42
Ti	0.00	0.01	0.00	0.00	0.00	0.01	0.01	0.01	0.61	0.49	0.76	0.19	0.61	0.52	0.61	0.55
Al	3.93	3.94	3.91	3.96	3.95	3.93	3.94	4.01	2.96	3.37	3.12	3.12	2.96	2.94	2.91	2.98
Cr	0.01	0.01	0.01	0.00	0.00	0.00	0.00	0.01	0.00	0.01	0.00	0.02	0.01	0.02	0.02	0.00
Fe^{+3}	0.07	0.05	0.09	0.04	0.06	0.07	0.06	0.00								
Mg	1.49	1.30	1.17	1.07	1.43	1.03	1.43	1.42	2.76	2.65	2.14	2.62	2.70	2.72	2.70	2.85
Ca	0.57	0.35	0.76	0.43	0.87	0.59	0.47	0.15	0.00	0.00	0.00	0.00	0.00	0.00	0.00	0.00
Mn	0.27	0.14	0.07	0.20	0.12	0.22	0.13	0.20	0.01	0.01	0.00	0.01	0.00	0.01	0.00	0.01
Fe^{+2}	3.70	4.26	3.97	4.34	3.68	4.21	4.05	4.38	1.83	1.72	2.08	2.42	1.93	2.18	2.05	1.78
Ni	0.00	0.01	0.01	0.00	0.00	0.00	0.00	0.01	0.01	0.00	0.00	0.01	0.01	0.00	0.01	0.01
Na	0.00	0.01	0.03	0.03	0.00	0.00	0.00	0.02	0.06	0.15	0.06	0.06	0.07	0.06	0.05	0.05
K	0.00	0.00	0.00	0.00	0.00	0.01	0.00	0.01	1.75	1.78	1.77	1.74	1.64	1.67	1.75	1.81
Total	16.02	16.04	16.02	16.04	16.06	16.03	16.02	16.10	15.40	15.47	15.27	15.66	15.34	15.54	15.46	15.47
Gro	7.54	4.12	10.29	5.93	12.78	7.84	6.02	1.96								
Pyr	24.73	21.54	19.59	17.66	23.45	17.02	23.56	23.12								
Spe	4.50	2.24	1.23	3.38	2.04	3.70	2.18	3.19								
Alm	61.30	70.47	66.43	71.88	60.21	69.64	66.57	71.43								

Minerals	Ternary feldspar														
Specimen	94t12			94t26			95t134			95t146			95t146		
Location	Pl	Or	Antiper	Pl	Or	Antiper	Pl	Or	Antiper	Pl	Or	Antiper	Pl	Or	Per
SiO_2	60.79	65.43	61.02	61.15	65.14	61.23	58.41	65.24	58.75	59.70	66.35	60.37	62.08	66.06	64.86
TiO_2	0.00	0.00	0.00	0.00	0.02	0.00	0.01	0.08	0.00	0.03	0.04	0.03	0.09	0.05	0.01
Al_2O_3	23.82	18.48	23.55	24.75	17.98	24.62	25.53	18.21	25.16	25.06	19.03	24.46	23.31	18.61	20.02
Cr_2O_3	0.00	0.00	0.00	0.00	0.00	0.00	0.01	0.00	0.01	0.00	0.05	0.01	0.048	0.04	0.04
MgO	0.03	0.00	0.00	0.00	0.01	0.00	0.00	0.00	0.00	0.00	0.00	0.00	0	0	0.00
CaO	5.81	0.06	5.52	6.91	0.13	6.77	8.33	0.06	7.92	7.44	0.18	6.72	5.476	0.067	1.69
MnO	0.04	0.00	0.04	0.00	0.00	0.00	0.03	0.00	0.00	0.02	0.00	0.02	0	0	0.00
FeO	0.04	0.00	0.04	0.03	0.00	0.03	0.01	0.01	0.01	0.10	0.01	0.09	0.041	0	0.01
NiO	0.02	0.00	0.00	0.00	0.03	0.00	0.00	0.04	0.00	0.00	0.07	0.01	0	0.008	0.01
Na_2O	8.15	1.69	7.83	6.74	1.46	6.64	6.60	0.86	6.31	6.22	4.25	6.02	8.195	2.751	4.38
K_2O	0.49	13.95	1.16	0.88	14.20	1.14	0.40	15.57	1.16	0.82	10.54	1.79	0.397	12.75	9.04
Total	99.18	99.61	99.15	100.47	98.96	100.43	99.34	100.08	99.33	99.41	100.53	99.52	99.56	100.3	100.07
O	8	8	8	8	8	8	8	8	8	8	8	8	8	8	8
Si	2.73	3.01	2.74	2.71	3.02	2.72	2.63	3.01	0.00	2.68	2.99	2.71	2.71	3.004	2.92
Ti	0.00	0.00	0.00	0.00	0.00	0.00	0.00	0.00	0.05	0.00	0.00	0.00	0.00	0.00	0.00

(*To be continued on the next page*)

(*Continued*)

Minerals	Ternary feldspar														
Specimen	94t12			94t26			95t134			95t146			95t146		
Location	Pl	Or	Antiper	Pl	Or	Antiper	Pl	Or	Antiper	Pl	Or	Antiper	Pl	Or	Per
Al	1.26	1.00	1.25	1.29	0.98	1.29	1.36	0.99	0.00	1.32	1.01	1.29	1.22	1.00	1.07
Cr	0.00	0.00	0.00	0.00	0.00	0.00	0.00	0.00	0.00	0.00	0.00	0.00	0.00	0.00	0.00
Mg	0.00	0.00	0.00	0.00	0.00	0.00	0.00	0.00	0.38	0.00	0.00	0.00	0.00	0.00	0.00
Ca	0.28	0.00	0.27	0.33	0.01	0.32	0.40	0.00	0.00	0.36	0.01	0.32	0.26	0.00	0.08
Mn	0.00	0.00	0.00	0.00	0.00	0.00	0.00	0.00	0.00	0.00	0.00	0.00	0	0	0.00
Fe^{+2}	0.00	0.00	0.00	0.00	0.00	0.00	0.00	0.00	0.00	0.00	0.00	0.00	0.00	0.00	0.00
Ni	0.00	0.00	0.00	0.00	0.00	0.00	0.00	0.00	0.55	0.00	0.00	0.00	0.00	0.00	0.00
Na	0.71	0.15	0.68	0.58	0.13	0.57	0.58	0.08	0.07	0.54	0.37	0.52	0.71	0.24	0.38
K	0.03	0.82	0.07	0.05	0.84	0.07	0.02	0.92	4.99	0.05	0.61	0.10	0.02	0.74	0.52
Total	5.01	4.98	5.01	4.96	4.98	4.96	4.99	4.99	55.05	4.95	4.99	4.96	5.00	4.99	4.99
Ab	69.78	15.47	67.06	60.56	13.39	59.62	57.54	7.72	55.05	57.22	37.68	55.27	71.37	24.61	38.64
Or	2.74	84.22	6.81	5.18	85.96	6.80	2.32	91.98	6.80	4.95	61.44	10.60	2.27	75.05	53.22

Minerals	Cordierite			Plagioclase				Spinel				Hypersthene	
Specimen	94t12	94t26	95t134	94t12	94t26	95t134	95t146	94t12	94t26	95t134	95t146	95t134	
SiO_2	48.60	48.53	49.14	44.57	43.52	44.49	44.90	0.06	1.73	0.09	0.11	51.75	50.65
TiO_2	0.02	0.00	0.00	0.00	0.00	0.00	0.00	0.03	0.01	0.04	0.04	0.18	0.05
Al_2O_3	32.52	32.80	32.49	34.02	34.49	34.43	34.58	59.16	57.01	58.14	58.46	1.56	2.66
Cr_2O_3	0.00	0.06	0.06	0.03	0.03	0.00	0.00	0.10	0.10	0.10	0.21	0.01	0.17
Fe_2O_3								1.81	1.30	2.22	1.82	0.00	0.00
MgO	8.88	8.82	8.28	0.01	0.00	0.00	0.02	4.79	5.59	4.72	4.68	19.06	17.68
CaO	0.01	0.01	0.00	18.55	18.71	19.04	19.02	0.04	1.02	0.17	0.10	0.11	0.15
MnO	0.16	0.19	0.22	0.00	0.07	0.04	0.00	0.05	0.04	0.35	0.45	0.26	0.21
FeO	7.99	7.86	8.40	0.60	0.09	0.33	0.17	31.90	30.46	32.43	32.67	27.34	27.60
NiO	0.00	0.09	0.00	0.02	0.02	0.01	0.00	0.09	0.03	0.07	0.10	0.02	0.00
ZnO								2.12	2.21	0.70	0.57		
Na_2O	0.07	0.11	0.06	1.02	0.72	0.81	0.88	0.04	0.0	0.00	0.00	0.01	0.00
K_2O	0.00	0.02	0.00	0.01	0.00	0.02	0.00	0.00	0.00	0.00	0.00	0.00	0.00
Total	98.26	98.50	98.65	98.83	97.64	99.16	99.56	100.18	99.53	99.01	99.20	100.33	99.16
O	18	18	18	8	8	8	8	32	32	32	32	6	6
Si	5.00	4.99	5.04	2.09	2.06	2.08	2.08	0.01	0.39	0.02	0.02	1.96	1.95
Ti	0.00	0.00	0.00	0.00	0.00	0.00	0.00	0.00	0.00	0.01	0.01	0.01	0.00
Al	3.94	3.97	3.93	1.88	1.92	1.89	1.89	15.66	15.27	15.57	15.61	0.07	0.12
Cr	0.00	0.01	0.00	0.00	0.00	0.00	0.00	0.02	0.02	0.02	0.04	0.00	0.01
Fe^{+3}								0.31	0.22	0.38	0.31	0.00	0.00
Mg	1.36	1.35	1.27	0.00	0.00	0.00	0.00	1.60	1.89	1.60	1.58	1.08	1.01
Ca	0.00	0.00	0.00	0.93	0.95	0.95	0.95	0.01	0.25	0.04	0.02	0.00	0.01
Mn	0.01	0.02	0.02	0.00	0.00	0.00	0.00	0.01	0.01	0.07	0.09	0.01	0.01
Fe^{+2}	0.69	0.68	0.72	0.02	0.00	0.01	0.01	5.99	5.79	6.16	6.19	0.87	0.89
Ni	0.00	0.01	0.00	0.00	0.00	0.00	0.00	0.02	0.01	0.01	0.02	0.00	0.00
Zn								0.35	0.36	0.12	0.10		
Na	0.01	0.02	0.01	0.09	0.07	0.07	0.08	0.02	0.01	0.00	0.00	0.00	0.00
K	0.00	0.00	0.00	0.00	0.00	0.00	0.00	0.00	0.00	0.00	0.00	0.00	0.00
Total	11.03	11.04	11.00	5.02	5.01	5.01	5.01	24.00	24.02	23.99	23.99	4.00	3.99

71.4% for orthoclase, and 24.4% for albite.

Biotites of peak granulite assemblages are mainly preserved in the garnet and kyanite prophyroblastes. The f/m rations of biotite in garnets are of 40 to 43 for all samples discussed (table 1), whereas f/m of biotites in matrix are of 38 to 48. The composition of biotites which are formatted in

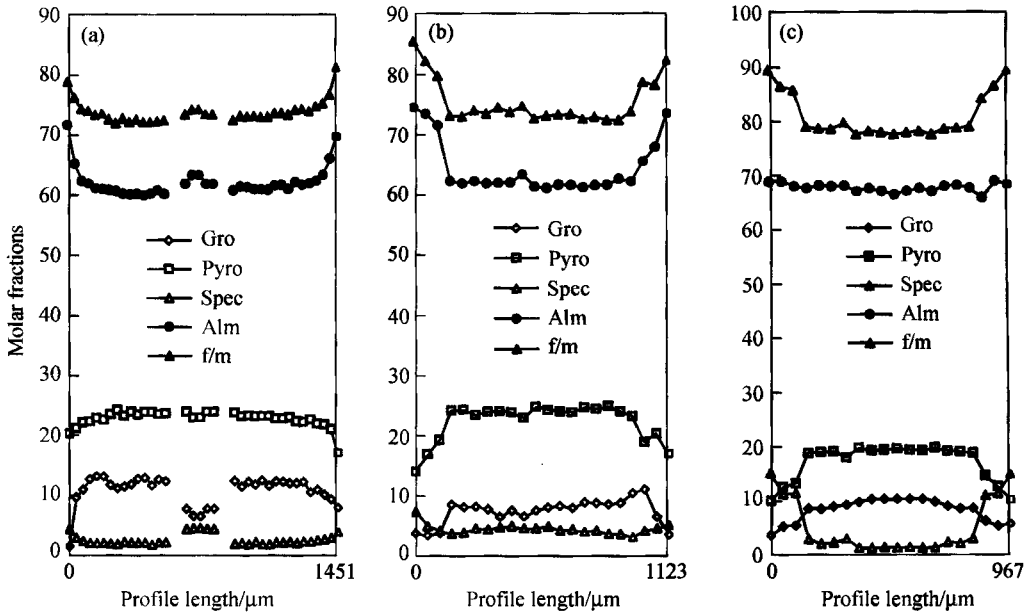

Fig. 3. Compositional profiles of almandine, pyrope, grossular, spessartine and f/m ratio of HP granulites from Namjagbarwa. (a) Cord + Q coronas at the rim of garnet (94T26). (b) An + Sp coronas at the rim of garnet (95T146). (c) Cord + Opx coronas at the rim of garnet (95T134)

the retrograde granulite assemblages of coronas are apparently different in different positions. Biotites within coronas rimming garnet prophyroblastes are FeO-rich, whereas closing the ilmenite are TiO_2-rich.

Cordierites, which occur in samples of 94T12, 94T26 and 95T134, are formatted in the retrograde granulite assemblages of symplectites around garnets and kyanites. They show yellow aureole when enclosing zircon. The compositions of cordierites show little differences between different samples and range from 8.28% to 8.82% for MgO, and from 7.86% to 10.26% for FeO.

Spinels, which occur in all samples discussed, are also formatted in the retrograde granulite assemblages of symplectites. These green spinels are mainly hercynite in which Cr/(Cr + Al) values range from 0.1 to 0.3, and f/m are range from 75 to 80.

Orthopyroxene, which only occurs in sample 95T134 in the retrograde granulite assemblages of Opx + Cord coronas mantling garnet or biotite prophyroblastes, are rich in FeO and MgO, poor in Al_2O_3 and CaO. The orthopyroxene are classified into hypersthene with end-members of Fs and En being range from 40% to 45% and 55% to 60% respectively. According the results of Hensen[8,9], the occurring of hypersthene results from the high MgO content in garnet.

4 Thermobarometric evaluation

Well-calibrated garnet-aluminum silicate-quartz-plagioclase (GASP) geobarometer[7] and garnet-biotite (GARB) geothermometer[10,11] can be applied to the peak assemblages of the granulite from Namjagbarwa. Ternary feldspars determined by integrated line scan analysis on the microantiperthite, garnets with high grossular on the electric-probe profiles, and biotites with lower f/m rations on the profiles in the same garnet have been selected for estimating the peak temperature and pressure.

The pressure and temperature, which have been interactively calculated using GASP and GARB, range from 793—836℃ and 1.6—18 Gpa (table 2). These P-T evaluations are generally the same as that of the peak granulite assemblages of grnet-clinopyroxene granulites which spatially co-exist with the garnet-kyanite granulites (750—850℃, 1.4—1.6 Gpa)[2].

Table 2 Thermobarometer evaluation results of garnet-kyanite granulite samples from Namjagbarwa

	T/℃	P/Gpa	T/℃	P/Gpa	T/℃	P/Gpa	T/℃	P/Gpa
	peak stage		retrograde stage					
	GARP-GASP		CAGS		TWQ		GARB-GASP	
94T12	793.96	1.62	689.64	0.70	594.74	0.56		
94T26	836.81	1.78	621.32	0.62	726.99	0.57		
95T134	822.74	1.80	658.35	0.63	630.1	0.60		
95T146	795.14	1.60					631.62	0.67

Ternary feldspar thermometer[5] has been used to estimate the peak temperature of garnet-kyanite granulites. These are of 810—920℃. Furthermore, the Mei = An + Cc reaction gives the same general temperture (760—850℃) for the peak granulite assemblages of scapolite + garnet + quartz in the calc-silicate granulites which spatially co-exist with the HP garnet-kyanite granulites[12]. Summing up the upper P-T evaluations, it is reasonable that peak granulite assemblages of garnet-kyanite formatted at the conditions of 1.4—1.8 Gpa and 750—850℃.

The P-T conditions for the retrograde assemblages have been estimated by the cordierite + sillimanite + garnet + quartz (CAGS) geothermobarometers[13] for the samples 94T12, 94T26 and 95T134 which range from 621 to 689℃ and 0.62 to 0.70 Gpa. Moreover, the general same P-T for the retrograde assemblages of Gt + Sill + Bi + Rt + Ilm + Cord + Q are computed using the TWQ software presented by Berman[14] range from 594—726℃ and 0.56—0.60 Gpa.

Sample 95T146 contain no cordierite, prohibiting used CAGS geothermobarometer. The P-T conditions for the retrograde assemblages of Sill + An + Sp + Ilm have been estimated using the GASP and GARB geothermobarometers which are of 631.62℃ and 0.67 Gpa. It is slight higher than the P-T results estimated by CASG geothermobarometers for the cordierite-in samples.

5 Metamorphic P-T-t path

The P-T-t path for the metamorphic evolution of the garnet-kyanite granulites from Namjagbarwa is shown in fig. 4. This path is constrained by the P-T conditions that have been discussed, mineral reactions inferred from the textures, petrogenetic grid for the peak and retrograde assemblages and the corresponding isotopic ages. It is a clockwise P-T-t path characterized by post-peak near-isothermal decompression (ITD).

The FMASCT grid can be developed using the TWQ software presented by Berman[14]. Peak metamorphic assemblages of Ky + Gt + Per + Rt + Q and the relic muscovite in kyanite elucidate rocks have crossed the reaction 2 at first (fig. 4). Lack of orthopyroxene in the peak granulite assemblages demonstrates that the rocks have not crossed the reaction 2. So the peak metamorphic conditions are constrained between reactions 3 and 2. The discovering of retrograde basic eclogites in the southwestern side of Namjagbarwa area indicate that some of the garnet-kyanite granulites should locate above the reactions of 5 at the peak pressure assemblages.

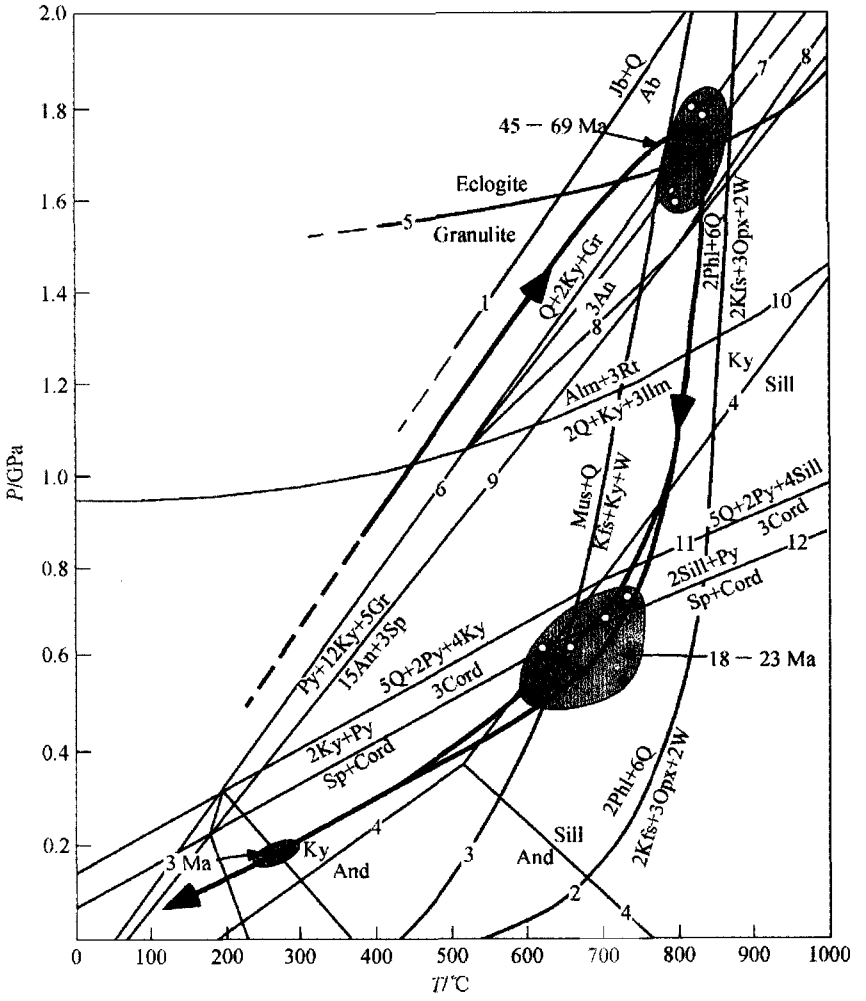

Fig. 4. P-T-t path and petrogenetic grid for the garnet-kyanite granulites from the Namjagbarwa. Reaction curves: 1, Holland (1980)[15]; 2, Vielzeuf & Montel (1994)[16]; 3, Thompson (1976)[17]; 4, Holdway (1971)[18]; 5, Green & Ringwood (1967)[19]; 6, petrogenetic grids developed using the TWQ software presented by Berman[14]; 7, 3Rt + 3Ky + 2Gr + Alm = 6 An + 3Ilm; 8, 2Alm + Gr + 6Rt = 3Q = 6Ilm + 3An; 9, 10, the same as that of 6.

Observed corona textures are consistent with the rocks cooling from peak conditions, and successively crossing the reactions marked as 4, 6—12 in fig. 4. The observation of anorthite coronas rimming garnet, anorthite + spinel symplectites mantling the kyanite porphyroblastes (fig. 2 (g), (j) and (m)) and ilmenite coronas replacing rutile show that the rocks have decompressed and reacted across reactions 6—10. With continuing pressure reduction, the granulites have reacted and across reaction 4, for the kyanite prophyroblastes were partially replaced by sillimanites at the rim (fig. 2 (a)) or completely replaced by prismatic sillimanites (fig. 2 (d)). At the last curtain, the second coronas within the presence of cordierites have been developed between the garnet and the sillimanite porphyroblastes. The Cord + Q and Cord + Sp symplectites on garnets and sillimanites suggest that the rocks have decompressed through and reacted across reactions 11 and 12.

The mineral textures of the Gt-Ky granulites also show the rocks have experienced rapid uplift. The quasi-stable kyanites coexist with cordierites and are replaced directly by sillimanites on their boundary (fig. 2(c) and (m)). Garnet porphyroblastes are unzoned except near their vary narrow rims (100—300 μm). All the retrograded minerals are preserved in the narrow coronas rimming garnet and kyanite porphyroblastes with a width of 100—300 μm. These minerals are very small with grainsize of 5—10 μm, and of anhedran shape, such as vermiform and embayed outline. All these textures show that they are of an unstable texture formed by rapid decompression (fig. 2(d), (f), (g), (h), (j), (k), (l) and (n)). The representative retrograde assemblages of Cord + Q, Cord + Sp ± An, An + Sp and Opx + Cord are typical assemblages for lower pressure granulites and the mineral reactions inferred from the texture are standard reactions for the granulites experienced ITD path[8,9,12,13].

Two kinds of garnet-kyanite granulites which have preserved peak mineral assemblages of Gt + Ky + ternary feldspar + quartz + rutile were selected for zircon U-Pb isotopic analysis. One is cordierite-absent sample (95T146) in its retrograde assemblages (An + Sp), in which kyanite has been well preserved and shows a triple junction texture of alkali microperthite. There are concordant U-Pb ages of (44.5 ± 4.93) Ma, (60.9 ± 1.95) Ma, (65.69 ± 1.53) Ma and (68.57 ± 1.7) Ma (fig. 5) for zircons. Another is cordierite-present sample (94T26) that gives a zircon U-Pb lower discondia intercept age of (22.6 ± 5.7) Ma (fig. 5). In view of reaction textures and retrograde degree from the peak metamorphic assemblages of the two samples for analysis, we prefer that the ages of 45—69 Ma generally represent that of formatting the peak granulite assemblages, and the age of 23 Ma indicates that of formatting of the retrograde granulite assemblages.

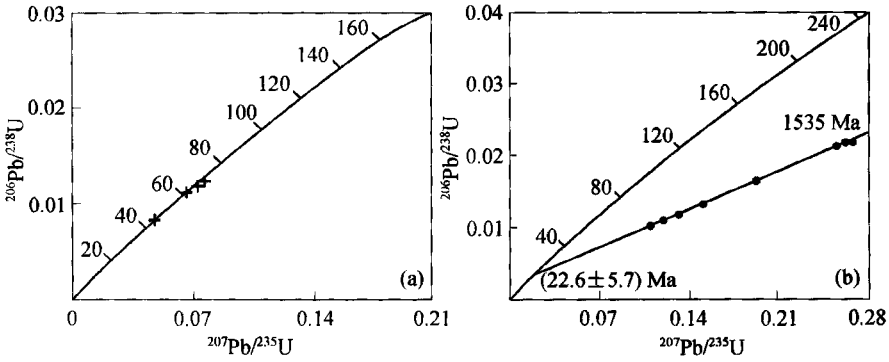

Fig. 5. Concordia diagram for zircon of two garnet-kyanite granulite samples from Namjagbarwa. (a) Concordant ages for zircon of cordierite-absent garnet-Kyanite granulite sample; (b) discondia age for zircon of cordierite-present garnet-kyanite granulite sample.

In addition, an age of (64.56 ± 1.29) Ma (fig. 6) which indicates the peak P-T metamorphic assemblages of garnet-clinopyroxene granulite is provided by $^{39}Ar/^{40}Ar$ plateau age of Clinopyroxene. These Garnet-Clinopyroxene granulites as lens exist within the garnet-kyanite granulites.

Moreover, an $^{39}Ar/^{40}Ar$ plateau age of (17.5 ± 0.3) Ma (fig. 6) has been determined on crust origin of the garnet-amphibole granite which is thought to have been formed during decompression. These garnet-amphibole granites are spatially intruded into the HP garnet-kyanite granulites.

A number of Fission-track ages are analyzed on apatites, zircons and sphenes of granulites and

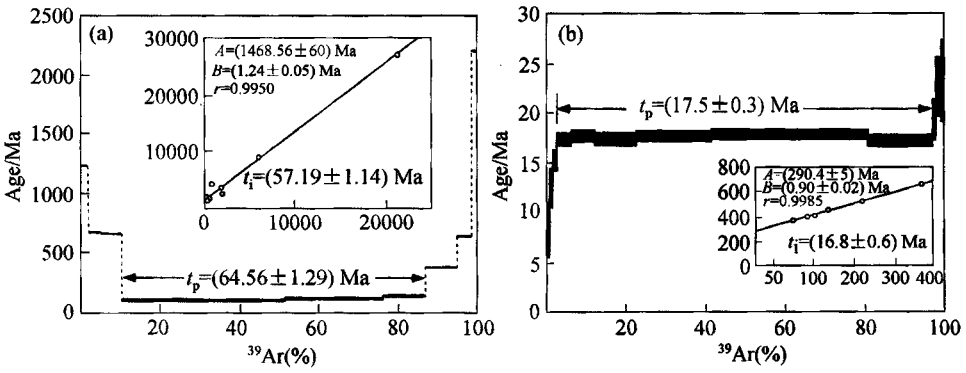

Fig. 6. $^{39}Ar/^{40}Ar$ age spectrum for clinopyroxene of garnet-clinopyroxene granulite (a) and for amphibole of garnet-amphibole granite (b).

granites from Namjagbarwa. These ages range from 0.16—3 Ma, indicating the cooling history of the retrograde assemblages outcropped[20,21].

6 Discussion on the geotectonic implications

The P-T-t path shown in fig. 5 indicates the formation of the peak granulite assemblages is at 750—850℃ and 1.4—1.8 Gpa which corresponds a depth of 70 km. The geothermal gradient deduced from the P-T conditions of the peak granulite assemblages is 14℃/km. This temperature is generally the same and the pressure is twice times than that of worldwide granulites ((800 ± 50)℃, (0.75 ± 0.1) Gpa) colligated by Harley[12]. The P-T conditions of the peak granulites from Namjagbarwa, which are approximately equal to the HP granulites from the Moldanubian zone of Lower Austria[22] and from North China[23—25], indicate that these rocks have been formed in an over-thickening orogenic belt. In the past, formation of granulite metamorphism has been inferred to be taking place in depth of the Himalayan orogenic belt[12]. What mechanism could result in the HP granulites rapidly outcropped in the EHS today?

Zhong Dalai & Ding Lin[26] have used a slab breakoff model for explaining the rapid exhumation of the HP granulites. According to this model, slab breakoff will occur with light continental lithosphere follows dense oceanic lithosphere into the subduction zone. Strong extension forces within the slab resulting from opposing buoyancy forces ultimately tear off the oceanic slab. A narrow rifting will occur with the oceanic falling down and the subducted continental lithosphere back uplifting. The subducted continental lithospheric crust can rapidly rise as buoyant sheets back into the crust due to their contrast in density with the surrounding mantle, resulting in the rapid exhuming of the HP granulite and even coesite-bearing eclogites. The resulting rift will be filled by hot, uprising asthenospheric mantle. This conductive heating will lead to partial melting of enriched metasomatic layers with the lithospheric mantle, producing alkaline, ultrapotassic, or calc-alkaline basalts. These will rise into the crust and result in the melting of crust, producing the intrusion of granitoids.

Both granitic and mafic magmatism synchronously and spatially occur within the HP granulites during the retrograde stage from Namjagbarwa. These mantle-derived gabbro, diecite, lamprophyre and carbonate and crust origin of garnet-amphibole granite are 8—18 Ma. So the slab-breakoff may be a reasonable model for explaining the rapidly exhumation of HP granulites and the formatting of bi-

modal magmatism in Namjagbarwa.

With the rebounding of the subducted wedge of the Indian Plate, the subduction zone migrated southward. MCT and MBT activated successively 26—18 Ma. The detachment faulting extensively developed during 25—22 Ma in southern Tibet and the Himalayas, resulting in the rapid uplift of the crystal series of Himalaya.

If the ages of peak granulite assemblages demonstrate that the collision of the Indian Plate with the Eurasian Plate at EHS is about 70 Ma ago, which is earlier than the wildspread receipting 45—50 Ma[27]. It would eliminate the scissors-collision model of colliding from the western Himalayan syntaxis beginning at about 50—60 Ma[28] then migrating to the eastern Himalayan syntaxis.

Acknowledgement The authors are grateful to Xu Ping, Han Xiuling, Zhang Liansheng, Li Damin, Sang Haiqing and Mike Murphy for assistance with sample analysis.

References

1 Ding Lin, Zhong Dalai, Pan Yusheng et al., Fission-track evidences for the Neocene rapid uplift of the eastern Himalayan systaxis, *Chinese Science Bulletin*, 1995, 40(16): 1497.
2 Zhong Dalai, Ding Lin, Discovery of high-pressure granulite from Namjagbarwa area, *Chinese Science Bulletin*, 1995, 40(14): 1 343.
3 Zheng Xilan, Chang Chenfa, Geotectonic characteristics of the lower Yarlung Zangbo River, *Geologic Sciences*, 1979, (2): 116.
4 Wang Tianwu, Ma Rui, The metamorphic characteristics of the Namjagbarwa area, southeastern Tibet, *Journal of Changchun University of Earth Sciences*, 1996, 26: 152.
5 Fuhrman, M. L., Lindsley, D. H., Ternary-feldspar modelling and thermometry, *American Mineralogist*, 1988, 73: 201.
6 Spear, F. S., Cheney, J. T., A petrogenetic grid for pelitic schists in the system SiO_2-Al_2O_3-FeO-MgO-K_2O-H_2O, *Contributions to Mineralogy and Petrology*, 1989, 101: 149.
7 Newton, R. C., Haselton, H. T., Thermodynamics of the garnet-plagioclase-Al_2SiO_5-quartz geobarometer, in *Thermodynamics of Minerals and Melts* (eds. Newton, R.C., Navrotsky, A., Wood, B. J.), New York: Springer-Verlag, 1981, 131—147.
8 Hensen, B. J., Green, D. H., Experimental study of the stability of cordierite and garnet in pelitic compositions at high pressure and tempertures, *Contributions to Mineralogy and Petrology*, 1973, 38: 151.
9 Hensen, B. J., Cordierite-garnet bearing assemblages as geothermometers and barometers in garnulite facies terranes, *Tectonophysics*, 1977, 43: 73.
10 Ferry, J. M., Spear, F. S., Experimental calibration of the partitioning of Fe and Mg between garnet and biotite, *Contributions to Mineralogy and Petrology*, 1978, 66: 113.
11 Berman, R. G., Mixing properties of Ca-Mg-Fe-Mn garnet, *American Mineralogist*, 1990, 75: 328.
12 Harley, S. L., The origins of granulites: a metamorphic perspective, *Geological Magazine*, 1989, 126: 215.
13 Wells, P. R. A., P-T condition in the Moines of the central Highlands, Scotland, *Journal of the Geological Society of London*, 1979, 136: 663.
14 Berman, R. G., Thermobarometry using muti-equilibrium calculations: a new technique, with petrological applications, *Canadian Mineralogist*, 1991, 29: 833.
15 Holland, T. J. B., The reaction albite = Jadeite + quartz determined experimentally in the range 600—1200℃, *American Mineralogist*, 1980, 65: 129.
16 Vielzeuf, D., Montel, J. M., Partial melting of metagreywackes, Part I. Fluid-absent experiments and phase relationships, *Contributions to Mineralogy and Petrology*, 1994, 117: 375.
17 Thompson, A. B., Mineral reactions in pelitic rocks, II. Calculation of some P-T-X (Fe-Mg) phase relations, *American Journal of Sciences*, 1976, 276: 425.
18 Holdaway, M. J., Stability of andalusite and the aluminum silicate phase diagram, *American Journal of Science*, 1971, 271: 97.

19 Green, D. H., Ringwood, A. E., An experimental investigation of the gabbro to eclogite transformation and its petrological applications, *Geochimica et Cosmochimica Acta*, 1967, 31: 767.

20 Schreyer, W., Abraham, K., Three-stage metamorphic history of a whiteschist from Sar e Sang, Afghanistan, as part of a former evaporite deposit, *Contributions to Mineralogy and Petrology*, 1976, 59: 111.

21 Ding Lin, Zhong Dalai, *Uplift Stage of Tibetan Plateau*, *Lithosphere Structure Evolution and Dynamics of Tibetan Plateau* (eds. Pan Yusheng, Kong Xiangru), Guangzhong: Guangdong Sciences & Technology Press, 1998, 379—400.

22 Carswell, D. A., O'Brien, P. J., Thermobarometry and geotectonic significance of high-pressure granulite: examples from the Moldanubian zone of the Bohemian Massif in Lower Austria, *Journal of Petrology*, 1993, 34: 427.

23 Zhai Mingguo, Guo Jinghui, Yan Yuehua, The discovery and primary study of the high-pressure from North China, *Science in China*, Ser. B, 1992, 35(12): 1325.

24 Ma Jun, Wang Renming, The discovery and geologic implications of the assemblages of kyanite + perthite from HP granulite zone of Xuanhua-Chicheng, China, *Acta Petrologic Sinica*, 1985, 11: 273.

25 Liu Liang, Zhou Dingwu, Wang Yan et al., Feldsic high-pressure granulites and its geologic implications of Qinling complex from eastern Qinling Mountains, China, *Science in China* (in Chinese), Ser. B, 1996, 26: 56.

26 Zhong Dalai, Ding Lin, Rising mechanism of the Tibetan Plateau, *Science in China* (in Chinese), Ser. B, 1996, 26: 289.

27 Dewey, J. F., Cande, S., Pitman, W. C., Tectonic evolution of the India/Eurasia collision zone, *Eclogae. Geol. Helv.*, 1989, 82: 717.

28 Beck, R. A., Burbank, D. W., Sercombe, W. J. et al., Stratigraphic evidence for an early collision between northwest India and Asia, *Nature*, 1995, 373: 55.